A Multi-Tiered Wavefront Sensor using Binary Optics

D.R. Neal, M.E. Warren, J.K.Gruetzner, T.G. Smith, R.R.Rosenthal
Sandia National Laboratories, PO Box 5800, Albuquerque, NM 87185-0601

T.S. McKechnie
POD Associates, Albuquerque, NM 87106

ABSTRACT

Wavefront sensors have been used to make measurements in fluid-dynamics and for closed loop control of adaptive optics. In most common Shack-Hartmann wavefront sensors, the light is broken up into series of rectangular or hexagonal apertures that divide the light into a series of focal spots. The position of these focal spots is used to determine the wavefront slopes over each subaperture. Using binary optics technology, we have developed a hierarchical or fractal wavefront sensor that divides the subapertures up on a more optimal fashion. We have demonstrated this concept for up to four tiers and developed the wavefront reconstruction methods for both segmented adaptive optics and continous wavefront measurement.

1 INTRODUCTION

Measuring the phase of an optical beam has many different applications. Phase measurement is used for surface metrology of optics, thin films, mechanical components and the characterization of a wide variety of light beams and lasers. It is extensively used in fluid mechanics to infer density distributions,[1] and has extensive applications in laser-beam propagation measurement and control, where the phase of the beam itself is an important parameter.[2–5] Numerous phase sensors have been designed, built and tested using various methods. The most common types are the interferometric (based on either shearing or spatial filtering) and Shack-Hartmann. For many applications these techniques provide adequate performance. However, in some circumstances, these techniques may be limited in bandwidth, and in their ability to measure the required parameters. We have developed a new type of wavefront sensor that may be used in these situations.

The Shack-Hartman wavefront sensor uses a series of small lenslets to dissect the incoming wavefront into a number of individual beamlets.[1–9] These beams are focused onto a detector to produce a measure of the focal spot position. The average angle of arrival of the wavefront across the lenslet aperture can be uniquely determined by dividing the measured spot position by the lenslet focal length. To determine the overall wavefront, these individual measurements must be pieced together to form a finite integration in two dimensions. This operation is generally referred to as wavefront reconstruction.[10–12] For real time systems it is often the most difficult and time-consuming operation and is prone to the introduction of error into the measurement process. It also places a limit on the eventual resolution of the Hartmann sensor for a given bandwidth, since it requires large matrix operations that must be performed in a digital computer. For example, current technology when applied to adaptive optics is limited by the computer speed to a few hundred channels in order to achieve the bandwidths required for atmospheric compensation. Hartmann sensors consist of a lenslet array, coupled with a detector array, data acquisition and analysis software. The lenslet array can be fabricated using discrete optics, binary optics, or by a number of other approaches.[13–15]

In the multi-tiered wavefront sensor we have used the basic approach of the Shack-Hartmann sensor, that of using spot position to provide tilt information over a subaperture, but have reorganized the subapertures in a more optimal configuration. The subapertures, instead of being organized into an array of orthogonal or hexagonal segments, are distributed throughout the entire aperture, so that samples from varying parts of the aperture are acquired simultaneously. This allows the wavefront to be sampled in a hierarchical manner, rather than on an orthogonal grid. This technique depends upon specialized optics that can only be fabricated using digital (or binary) optics technology. This technique lends itself well to hierarchical control of adaptive optics.[16,17]

We will present a description of the multi-tiered concept, wavefront reconstruction analysis techniques, the binary optics fabrication methods, a model that uses linear superposition of analytic solutions to calculate far-field diffraction for this geometry, and the results of an adaptive optics brassboard experiment.

SPIE 2201-133, MAr 12-18, 1994.

DISCLAIMER

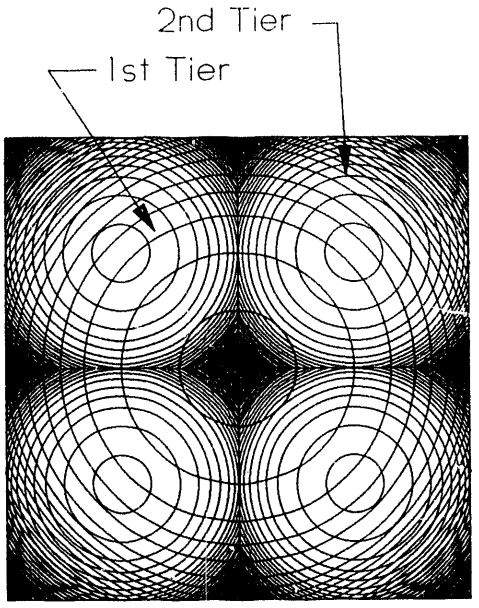

Figure 1: Two-tier lens system. Light from the entire aperture focused to a spot in the center of the field, in addition to the four focal spots from each quadrant.

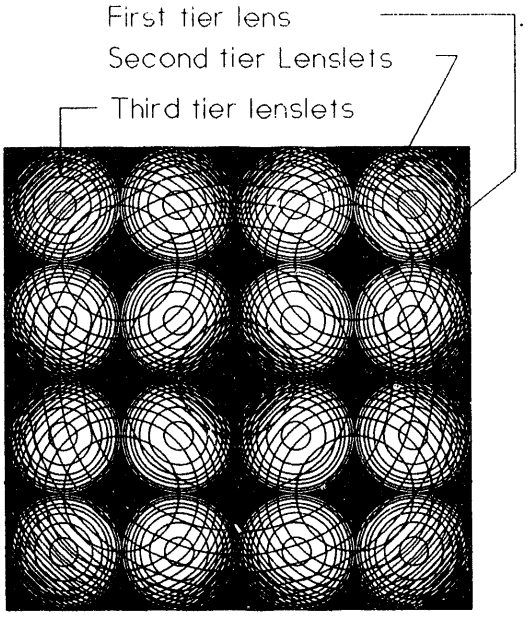

Figure 2: Three-tier lenslet array.

2 MULTI-TIERED CONCEPT

2.1 Description

The sensor uses a hierarchical scheme for acquiring the information about the wavefront. This allows information to be obtained with different levels of detail over the entire aperture simultaneously. The information is obtained in a manner similar to Hartmann sensing, by observing shifts in the position of a focal spot on a detector, but the focal spots move in response to the wavefront slope over different portions of the aperture. Each level in the hierarchy provides information on additional orders of wavefront slope.

Figure 1 depicts a typical arrangement for a two-tier system. In this sensor there are two independent sets of lenses. The first lens tier gathers light from the entire aperture and focuses it to a single spot in the center of the array. The second tier splits the aperture into four separate regions, with each region focused to the center of that region. These two tiers sample the same aperture using one of two techniques: faceted sampling or diffractive sampling. A similar method is followed for a three-tier system, four-tier and so on. An example of a three-tier system is presented in Figure 2.

There are two basic ways that this information is utilized. The measured derivatives of the wavefront over different subapertures can be used for direct computation of a series expansion of the wavefront, or the information can be used in a hierarchical control scheme to provide feedback for adaptive optics.

2.2 Aperture Multiplexing

There are basically two different techniques for designing these elements: diffractive (or computer generated hologram) and segmented aperture multiplexing. In the diffractive case, a series of computer generated holograms are constructed which diffract the light into the appropriate order. These can be fabricated using binary optics technology. The design process requires detailed calculations of the optical fields by the elements of the diffraction grating. Multiple level grating profiles can be used to increase the efficiency. This technique has the advantage that a simultaneous sample of the entire aperture can be acquired. However, the design requires sophisticated physical optics modelling. It is extremely difficult for the designer to intuitively choose grating elements which will produce the required results. While this type of design is feasible,[18] there is another, simpler technique available.

In the segmented aperture multiplexing approach, the entire aperture is broken up into a series of small segments. These segments are arranged in a regular grid

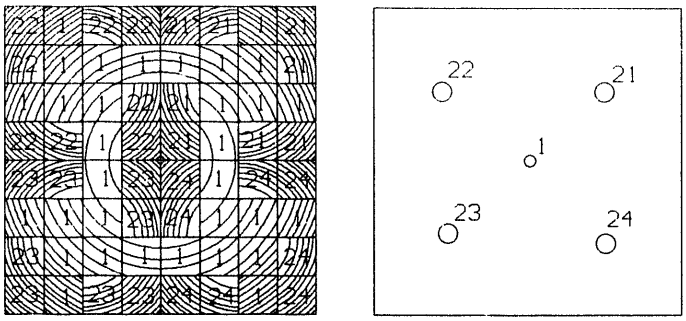

Figure 3: Two-tier lens arrangement for segmented aperture multiplexing using 16 segments per quadrant

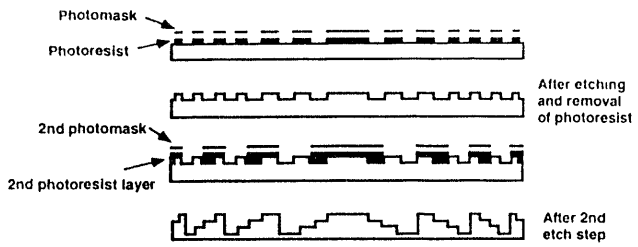

Figure 4: Fabrication steps in making a four phase level binary optical element.

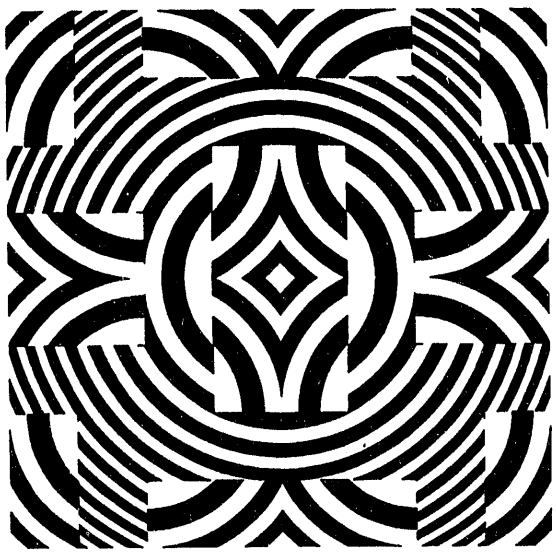

Figure 5: First mask layer layout for two-tier lens. The design is for a 25 mm focal length, 1 mm diameter lenslet array.

pattern to provide samples of the desired aperture. If these samples are small enough, then they may be focussed to different spots on the detector and the overall diffraction pattern is the coherent sum of all the individual segment apertures. This is depicted in Figure 3, which shows the arrangement for a two-tier lens. For this lens, the segments are 1/8 mm across, thus each quadrant has sixteen samples. For the first lens that we have constructed, one half of the light is partitioned into the central focus, and the other half divided among the four quadrant focuses. While this is not an optimum configuration, it is simple to design and construct and served as a pathfinder for design, fabrication and testing.

The drawback of segmented aperture multiplexing is that diffraction from the pattern of segments can interfere with the desired results. One must carefully select the design with this idea in mind. We have found that a random distribution of small segments, uniformly distributed throughout the larger subaperture gives good results. Several examples of the far-field patterns are presented Section 5.

3 FABRICATION

Fabricating the segmented-aperture lenslet arrays in these sensor designs would be nearly impossible without using binary optics technology. Binary optics was developed by Lincoln Laboratories researchers[19] as a sequential fabrication process for optical kinoforms or phase-only relief holograms that utilizes microlithographic processing technology. The process consists of repeated mask and etch steps to produce a phase profile as shown in Figure 4. For steep profiles, the etch depth can be limited by extracting the 2π phase factors from the profile to form a Fresnel lens structure. The term "binary optics" comes from the fact that N microlithographic steps in the process produces a phase profile with 2^N phase-steps. Because all of the features, including the lens boundaries, are defined microlithographically, the sizes and positions of the various lenslet segments that go with each tier can be determined by the optical designer and fabricated without regard for any of the usual optical fabrication limitations. The diffraction efficiency of the lenslet array is limited by the number of the phase-steps fabricated into the profile and the fabrication tolerances, particularly the alignment accuracy of the mask layers.[20]

The lenslet arrays for the multi-tiered wavefront sensors were fabricated in fused silica with four mask steps to yield structures with 16 phase levels. The masks have progressively finer features to define the profile. Figure 5 shows one photomask layer for a two-tier device and Fig-

Figure 6: First mask layer layout for four-tier lens. The design is for a 75 mm focal length, 4 mm diameter lenslet array.

ure 6 shows a photomask pattern for a four-tier lenslet array. The individual segments of the mask are rectangular regions from various lens masks that are then assembled into the final pattern. The mask layout is performed with a computer-aided-design (CAD) package for integrated circuit mask design. The CAD package includes a programming language. Programs we have written allow automatic generation of the lens mask by solution of the phase function of a simple lens for zone boundaries of each phase level. Rectangular segments of these lens masks can then be assembled by cut-and-paste in the CAD package. Since all of the lens segments in the array are designed for the same focal length, the first tier, which samples the entire aperture and produces one focal spot, is the fastest lens in the design and has smaller phase-step boundaries as one can see in Figure 5. The higher tier lenses have slower elements, since they sample a smaller part of the aperture. Because the photolithography process we are using has a limited resolution of approximately one micron for the smallest printable feature, the faster lenses may have lines near the edge of the pattern that will not print and these are eliminated from the photomask layer design. This produces a fall-off in the diffraction efficiency from those areas, but that can be compensated for by adjusting the aperture area devoted to that tier.

We start the processing with fused silica flats and spin-coat photoresist on one surface. The resist is exposed in a contact printer or mask aligner that allows precise alignment of subsequent layers to the first. The developed resist pattern is then transferred to the fused silica surface by reactive ion etching with a CHF_3 and O_2 plasma. This is an rf-discharge plasma process that allows anisotropic etching of the fused silica so that the boundaries and straight side walls of the photoresist pattern are faithfully reproduced into the fused silica. A wet etching process would not work for the smaller features because it would be isotropic and etch laterally at the same rate it is etching downward. The first mask used is actually the one with the smallest features, as depicted in Figure 4 because the smallest features are best reproduced on the most planar surface. After the etching is complete, the resist is removed and the process repeated with the next photomask. Each subsequent step is etched twice as deep as the first. The final fabrication step is to deposit an evaporated metal layer around the perimeter of the array to act as an aperture stop for the array.

4 WAVEFRONT RECONSTRUCTION

The multi-tiered wavefront sensor may be used to derive the wavefront in a variety of ways, depending upon the intended application.

In closed loop control of segmented adaptive optics, the information may be used to drive tip/tilt steering mirrors in combination with a far-field sensor. A recursive wavefront reconstruction algorithm may be used for continuous wavefront reconstruction.

4.1 Segmented adaptive optics applications

In a segmented adaptive optics system, such as shown in Figure 7, the multi-tiered wavefront sensor may be used to provide independent information on tip/tilt of each segment along with combined beam information from two or more segments. By matching the subapertures to the smallest tier size, the lowest level provides an independent measurement of the tip/tilt for each segment. This is exactly analogous to a Shack-Hartmann sensor for each segment. Since each segment is independent of every other segment, it is straightforward to close the loop around tip/tilt for each segment independently. This greatly simplifies the control process, since all the loops are closed in parallel and no cross-coupling is present.

The coupling comes about through the piston phase. Once all of the segments have the appropriate tip and tilt, they must each be moved in piston to minimize the phase differences from edge to edge. This is where the

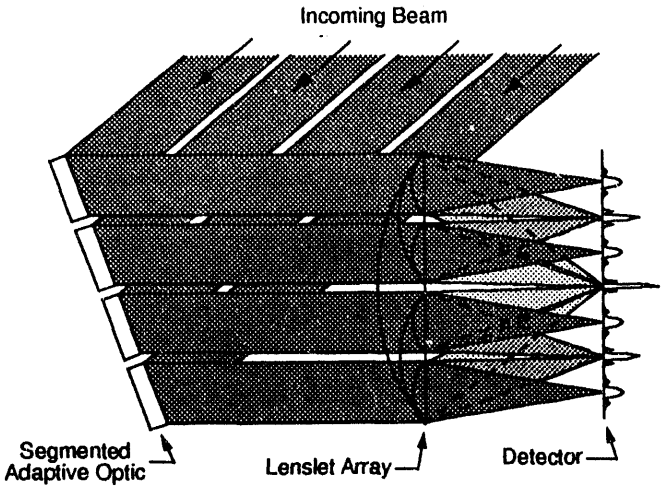

Figure 7: Segmented adaptive optical system with multi-tiered wavefront sensor for hierarchical control

various tiers of the sensor come into play. Each of the mirror segments is combined together in a group of four, with many groups of four making up the whole aperture. For example, for a 64 segment mirror (8×8), there are 16 groups of four in the third tier. The focal spots of this tier represent the combined beams from each group of four. Using far-field wavefront sensing or optimization techniques the segments can be adjusted in each group to provide optimum phase. This operation is performed in parallel throughout the next highest tier (3 in our example). Once these groups have been phased, groups of four groups are combined together in the next lowest tier (2 in the example). Each of these groups represents the combination of 16 segments. However, each group of four is already phased, so entire groups are adjusted to optimize the phase. This procedure continues until the lowest tier is reached, in which case the phase is of each quadrant is adjusted to optimize the central far-field intensity.

While we have described a situation where the tiers consisted of 2×2 groups of four mirror segments each, the concept can be applied to other numbers of mirrors in each group, and to a different number of groups in each tier. We have considered primarily square aperture shapes, although other shapes are amenable to this process.

The most serious drawback to this technique is the necessity to perform phasing based on far-field measurements. This can be an extremely difficult process that is full of redundancies and spurious local maxima. We have devised several schemes for dealing with this problem that will be outlined below.

The most straightforward set of schemes are based on some type of optimization.[21–23] One simply adjusts the mirror piston positions until the maximum center intensity (or other merit function) is obtained. There are numerous algorithms for performing this operation including binomial search, simplex,[21–24] and genetic algorithms.[18] The biggest drawback to these schemes is the dynamic nature of adaptive optics. Optimization schemes work well for static alignment problems, but often have trouble adapting to changing input conditions. There have been some recent modifications to some of these schemes to allow a more dynamic calculation,[24] although we have not yet tested them.

Another method of determining the piston phase of four beams is to combine them two by two and compare the resulting interference patterns. Pair wise interference patterns can be created using a slightly different binary optic. Instead of focusing the light in the middle of a group of four segments, the light is focussed between each pair of adjacent subapertures. This leads to the creation of an interference pattern between the top two segments, the right two, the bottom two and the left two. The phase of each pair is calculated from the fringe pattern of the interferogram between them, and the overall phase is determined by summing the relative phases around the loop (with one element fixed as a reference). Since there are four phase calculations and only three independent parameters, the additional measurement may be used for noise reduction or simply may be ignored. This scheme fits into the same hierarchy as the far-field phasing scheme since groups of segments can be compared using interference patterns in the next tier.

4.2 Continuous wavefront error measurement

For measuring or controlling the phase of a continuous system, the wavefront reconstruction is considerably simpler than alternative techniques and does not rely on interpretation of interferograms or far-field phasing. The centroid position of the spots from the various tiers is sufficient to completely describe the wavefront in a Taylor series (or other polynomial) expansion. In this case the centroid location of the central spot (1st tier) is used to determine overall tip and tilt of the whole wavefront. The differences in the measured tilt in the next tier can be used to measure the curvature of the wavefront over the whole aperture. The next tier is used for the third derivative terms, etc.

An optical phase front can be described as a Taylor series expansion in terms of the derivatives evaluated at

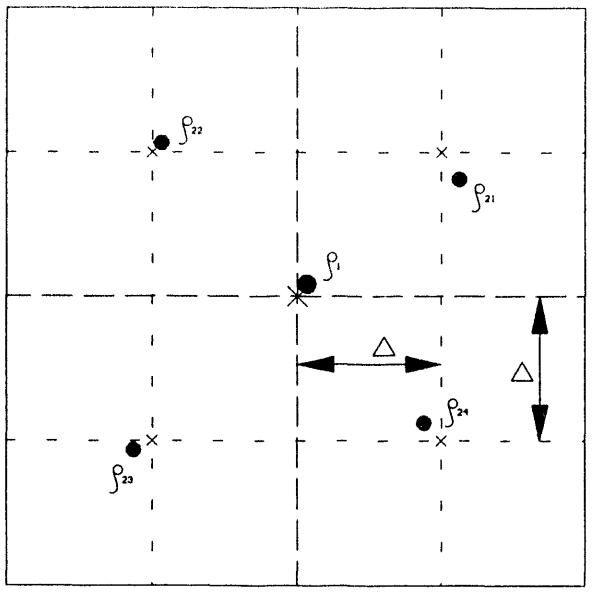

Figure 8: Far-field geometry for a multi-tiered lenslet array. The spots ρ_{ij} are the focal spots from the various tiers and are labeled by their tier and quadrant.

the center of the aperture:

$$\phi(x,y) = \phi(0,0) + \left.\frac{\partial\phi}{\partial x}\right|_{(0,0)} x + \left.\frac{\partial\phi}{\partial y}\right|_{(0,0)} y + \frac{1}{2}\left.\frac{\partial^2\phi}{\partial x^2}\right|_{(0,0)} x^2 + \frac{1}{2}\left.\frac{\partial^2\phi}{\partial y^2}\right|_{(0,0)} y^2 + \frac{1}{2}\left.\frac{\partial^2\phi}{\partial x\partial y}\right|_{(0,0)} xy + \frac{1}{2}\left.\frac{\partial^2\phi}{\partial y\partial x}\right|_{(0,0)} yx + \cdots \quad (1)$$

with the general expansion given by:

$$\phi(x,y) = \sum_{n=0}^{M}\left[\sum_{i=0}^{n}\frac{x^{(n-i)}y^i}{i!(n-i)!}\left.\frac{\partial^{(n-i)}\phi}{\partial x^{(n-i)}}\right|_{(0,0)}\left.\frac{\partial^i\phi}{\partial y^i}\right|_{(0,0)}\right] \quad (2)$$

Thus to measure the phase $\phi(x,y)$ over the aperture, it becomes a matter of measuring the derivatives evaluated at $(0,0)$. The first tier allows a direct determination of $\partial\phi/\partial x$ and $\partial\phi/\partial y$ from the position in the focal plane of the centroid of the focal spot $\hat{\rho}_1$ depicted in Figure 8.

$$\frac{\partial\phi}{\partial x} = \frac{\hat{\rho}_{1_x}}{f} \quad (3)$$

with $\hat{\rho}_{1_x}$ determined from

$$\hat{\rho}_{1_x} = \frac{\sum_i x_i s_i}{\sum_i s_i} \quad (4)$$

where s_i is the measured intensity values of the pixels near the central focal spot.

It is only slightly more difficult to produce the next higher order set of derivatives. They can be calculated from the differences of the first order derivatives in each quadrants. The next tier allows ready measurement of the derivatives evaluated at the center of each quadrant:

$$\left.\frac{\partial\phi}{\partial x}\right|_{(\Delta,\Delta)} = \frac{\hat{\rho}_{21_x}}{f} \quad (5)$$

where $\hat{\rho}_{21}$ is the spot position of the second tier, first quadrant, which is centered at (Δ,Δ). The second derivative can be measured by finite differencing the first derivatives in the adjacent quadrants

$$\left.\frac{\partial^2\phi}{\partial x^2}\right|_{(0,\Delta)} = \frac{\left.\frac{\partial\phi}{\partial x}\right|_{(\Delta,\Delta)} - \left.\frac{\partial\phi}{\partial x}\right|_{(-\Delta,\Delta)}}{2\Delta} \quad (6)$$

This finite difference is not in fact an approximation, since the centroid measures exactly the average tilt over the entire subaperture.[25] To determine the second derivatives at the center of the aperture, the upper and lower quadrants are averaged:

$$\left.\frac{\partial^2\phi}{\partial x^2}\right|_{(0,0)} = \frac{\left.\frac{\partial^2\phi}{\partial x^2}\right|_{(0,\Delta)} + \left.\frac{\partial^2\phi}{\partial x^2}\right|_{(0,-\Delta)}}{2} \quad (7)$$

The y derivatives and cross terms are calculated in a similar manner. This method of calculating the higher order derivatives is easily extended to the next higher tier for calculation of the third order terms and to the fourth tier for the fourth order terms and so on.

4.3 Applications

This device has a number of different applications. It provides an efficient means of estimating the wavefront from a few centroid measurements. For real time adaptive optics systems where the wavefront must be reconstructed rapidly, it can save precious computer time. For example, a four-tier system can estimate a fourth order (x and y) wavefront error with 21 operations, compared to 4000–250,000 using an efficient Shack-Hartmann wavefront reconstruction. Furthermore, the information can be carried through the control system in the form of a few coefficients, rather than a table of random data. Fewer numbers need to be passed back and forth throughout the system.

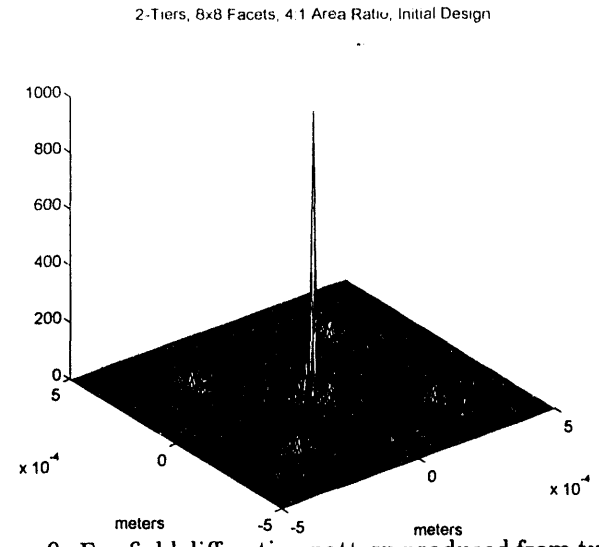

Figure 9: Far-field diffraction pattern produced from two-tier lens with segmented aperture multiplexing. The facet pattern used is shown if Figure 3.

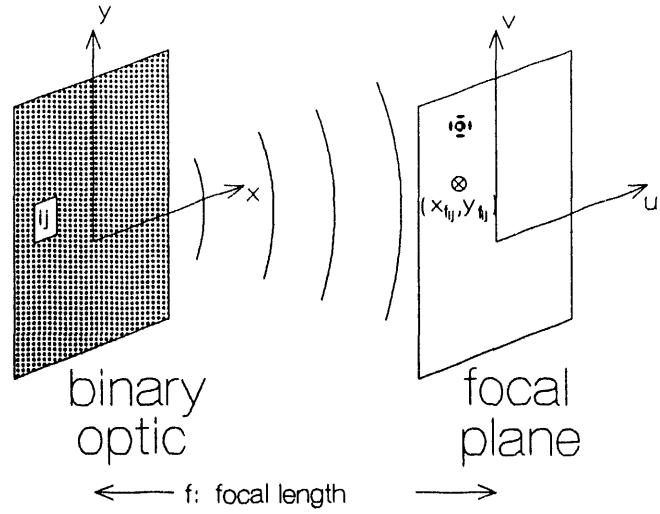

Figure 10: Model calculation geometry. Diffraction from each facet ij is summed to provide the appropriate intensity pattern at $x_{f_{ij}}, y_{f_{ij}}$.

Since this wavefront sensor makes series expansions of the wavefront readily available, it will be useful for measuring aspheres or other surfaces with rapid turnaround. This may be extremely useful in automated manufacturing or testing applications. Aspheric lens surfaces, disk drive platens, thin sheets or other processes can be monitored in real time with a two-dimensional sensor.

5 MODELING

One of the potential problems with segmented aperture multiplexing is diffraction from the small segments. Thus it is extremely important to be able to model the far-field diffraction process during the design of the lenslet array. We have used two approaches in this modelling: Fourier optics using fast Fourier transforms (FFTs), and linear superposition of analytic solutions. Since this problem looks like a large number of very similar aperture segments (or *facets*), we have found that the latter approach is more efficient in some situations. An example of the far-field diffraction pattern from the two-tier lens described in previous sections is presented in Figure 9. This model was developed using MATLAB.[26] The action of each facet of the binary optic is modeled as a portion of the lens to which it belongs. The model accounts for the average wavefront tip, tilt, and piston over the facet area, and then models the diffraction pattern produced by that facet. The far-field diffraction effects on the complex amplitude resulting from the facet aperture are centered about the lenslet focus position, which is shifted by the average wavefront tip/tilt across the facet.

The complex amplitude arising in the far-field from a rectangular aperture is a sinc function. Thus we can calculate facet diffraction effects analytically rather than using Fourier transforms. The appropriate phase factor is added to account for the lenslet position relative to the focus position and segment input tip/tilt and piston. Figure 10 shows the geometry of the analytical diffraction problem. For a single facet ij this results in the following solution as a function of image plane position:

$$\tilde{E}_{ij}(u,v) = \sqrt{I_{ij}}\,\frac{ab}{i\lambda f}\,\exp(2\,\pi\,i\,\varepsilon_{ij}) \times \tag{8}$$
$$\operatorname{sinc}\left(\frac{\pi a(u - f\,\theta_{ij} - x_{f_{ij}})}{\lambda f}\right) \times$$
$$\operatorname{sinc}\left(\frac{\pi b(v - f\,\psi_{ij} - y_{f_{ij}})}{\lambda f}\right) \times$$
$$\exp\left[2\,\pi\,i\frac{(u - f\,\theta_{ij} - x_{f_{ij}})\,(x_{ij} - x_{f_{ij}})}{\lambda f}\right] \times$$
$$\exp\left[2\,\pi\,i\frac{(v - f\,\psi_{ij} - y_{f_{ij}})\,(y_{ij} - y_{f_{ij}})}{\lambda f}\right]$$

where $\sqrt{I_{ij}}$ is the input wave amplitude over each facet, a, b are the horizontal and vertical facet widths, u, v are the image plane coordinates, x_{ij}, y_{ij} are the coordinates of the center of the i, j-th facet. $x_{f_{ij}}$, $y_{f_{ij}}$ are the coordinates of the focus point, f is the lenslet focal length,

ε_{ij} is the average wavefront advancement (piston) over the facet, and θ_{ij}, ψ_{ij} are the average wavefront tip and tilt. The resulting set of solutions is coherently added to form the solution for the entire array of facets. In two dimensions,

$$I(u,v) = \left| \sum_{i=1}^{N} \sum_{j=1}^{M} \tilde{E}_{ij}(u,v) \right|^2 \qquad (9)$$

This method relies on the principle of linear superposition to calculate the fields from the addition of many separate solutions. It has a number of advantages in some situations over the more conventional Fourier optics approach. Within the limitations imposed by discretizing the incoming wavefront over the input facets, the diffraction calculation from each facet is exact at each field point (u,v). Thus the sampling requirements on (u,v) are only such that a sufficient quality view is obtained. We have typically chosen a fairly large number of points (129×129) to have well resolved plots, but for other calculations it is only necessary that the Nyquist sampling condition be observed. Even if (u,v) were to be greatly undersampled, the calculation is exact at each point. No effects of aliasing are present. The FFT approach, on the other hand, places strict requirements on the sampling of both the near and the far-field. Guard bands must be used to avoid imposing periodic boundary conditions. This often leads to very large FFTs (512×512 are not unusual). For our typical problems the linear superposition model runs a factor of ten times faster than the FFT approach.

Model results show clearly that an increase in the number of lenslet facets reduces diffractive effects (as long as the facets remain large when compared to the wavelength). In the limit, where an infinite number of infinitesimally small facets are used, each lenslet samples the wavefront uniformly at an infinite number of points, so that there is no diffraction other than that expected from Huygen's-Fresnel diffraction from the lenslet aperture. Figure 11 shows the result of modeling a two-tiered binary optic composed of 64 (8×8) facets. Figure 12 shows the result of a two-tiered optic containing 256 (16×16) facets. Note the reduction in energy outside the main peaks in Figure 12.

The arrangement of the facets is also found to be important. In both of the above cases, the facet arrangement within each quadrant was randomly chosen. Figure 13 shows an 8×8 array with the facets laid out in a checkerboard pattern. Much more energy is deposited outside the main lobes. The model clearly shows that this design, although simpler in concept and easier to produce

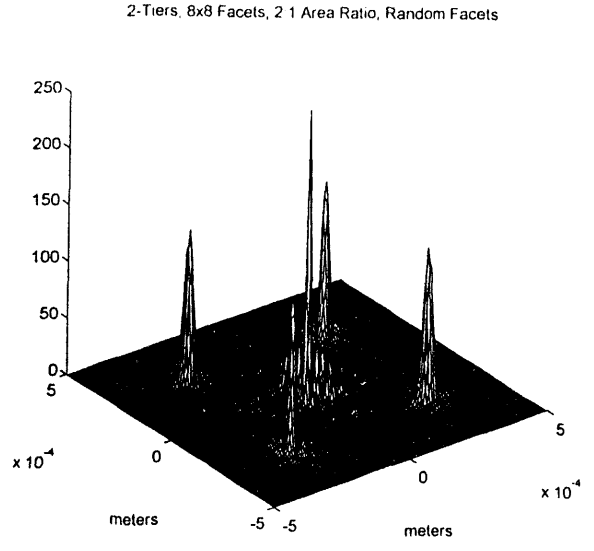

Figure 11: Model of image plane intensity pattern from a two-tiered binary optic composed of an 8×8 array of random facets.

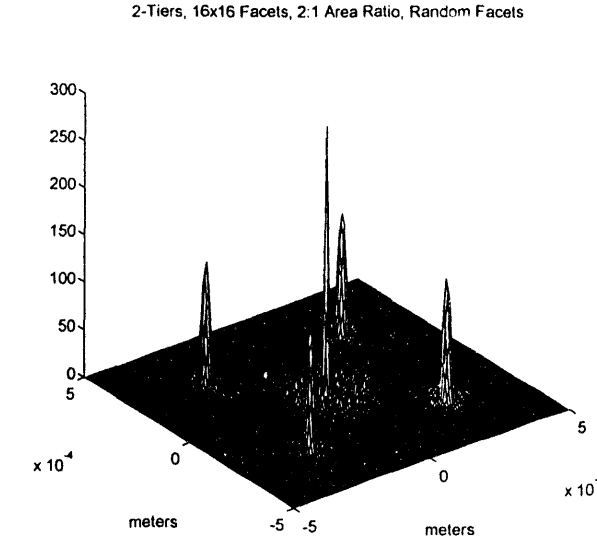

Figure 12: Model of image plane intensity pattern from a two-tiered binary optic composed of a 16×16 array of random facets.

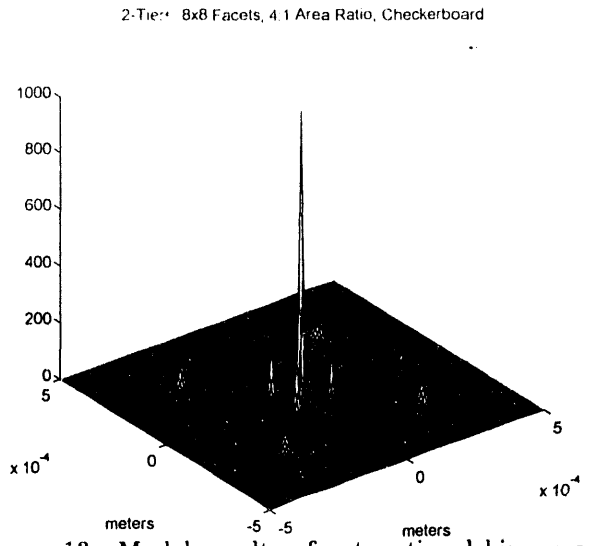

Figure 13: Model results of a two-tiered binary optic,

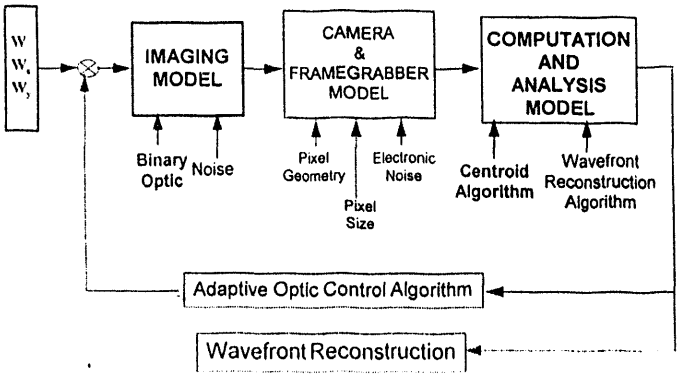

Figure 14: Multi-tiered wavefront sensor model block diagram. Reduced-intensity items are future additions.

than the others, is to be avoided.

Since we have implemented this program in MATLAB, a vector oriented calculation language, it is very easy to incorporate other elements in the calculation. For example, we are presently implementing the centroid calculations of Equation 4. With these calculations we expect to be able simulate the entire wavefront reconstruction process described in Section 4 and compare results to the input wave. We have several parts of this model working presently, but have not yet finished a complete comparison.Figure 14 shows some of the elements that we are planning to incorporate into this simulation.

6 ADAPTIVE OPTICS BRASSBOARD EXPERIMENT

One impetus behind this work is a brassboard experiment to demonstrate the combination of laser beams. Figure 15 depicts the major elements of this experiment. We are currently attempting to coherently phase four beams together. The initial brassboard experiment consists of a beam expander, beam dissector, adaptive optic, Shack-Hartmann wavefront sensor, far-field detector, and far-field imaging camera. We have demonstrated closed loop control of the wavefront tip/tilt using the Shack-Hartmann sensor, and far-field phasing using optimization from the far-field intensity sensor. While the discrete Shack-Hartmann sensor works well for the small number or mirrors that we are currently using, it becomes unwieldy when the number of beams is expanded to 64 or 256.

By using the multi-tiered wavefront sensor, we can replace most of the discrete optics with a single element. Each quadrant of the multi-tiered wavefront sensor is mapped to an image of the adaptive optics segment. This allows the tip/tilt of that segment to be measured from the focal spot position on the detector array. The loops can then be closed around this signal, instead of the signal from the separate Shack-Hartmann sensor, thus eliminating the need for the added complication of that optic and its mount. The center spot in the multi-tiered wavefront sensor image is the combined spot of all four beams. The far-field optimization and control schemes can be applied based on the information in this region. This eliminates the need for the discrete far-field sensor. In this way, most of the optics and mounts on the optical table can be replaced with a single binary optic. This optic can readily be expanded to a larger number of beams by scaling the adaptive optic.

Figure 16 shows a series of images obtained from the multi-tiered wavefront sensor. The four Shack-Hartmann spots are visible, and as they are driven into the center in each successive figure, it is evident that the center spot is growing in intensity. At this point the phasing algorithms are rather crude, using simple optimization schemes. We are working on the development of more sophisticated schemes that would work on four mirrors in real time. Once these are worked out, the hierarchical nature of the multi-tiered wavefront sensor lends itself well to hierarchical control of the adaptive optic. In this way, only four mirrors need ever be phased from the far-field. This greatly simplifies the control process, allowing for significant decoupling of the variables. (All of the tip/tilt is completely decoupled from the beginning). For a fixed

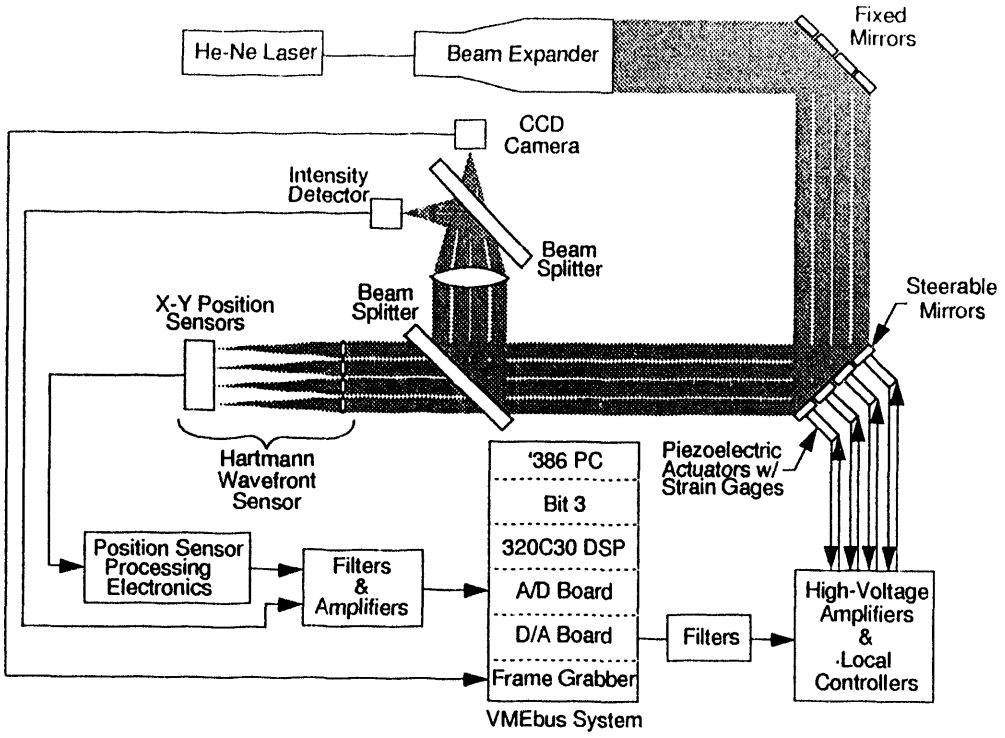

Figure 15: Beam combining brassboard layout.

control computer speed, where the wavefront reconstruction time is deemed to dominate, the scaling as a function of the number of degrees of freedom is shown in Figure 17. Depending on the number of tiers, significant improvement in attainable bandwidth are possible with this technique.

7 CONCLUSIONS

The use of binary optics has allowed us to construct unique optical elements that could not be fabricated with any other method. We have taken advantage of this to construct a novel wavefront sensor that has unique applications. The multi-tiered sensor, by using light from all portions of the aperture uses the structure of the light itself on the focal plane to form the appropriate information necessary for efficient wavefront sensing. The mathematics has been developed to support wavefront reconstruction both for continuous wavefronts and for closed loop control of segmented adaptive optics. We have fabricated several devices and the modeling and test results are in good agreement. We plan to continue the development of the hierarchical control concept using the multi-tiered wavefront sensor to a larger number of mirrors. We are currently pursuing plans for an 8×8 segmented deformable mirror, which would allow testing of the hierarchical control scheme to four tiers.

8 ACKNOWLEDGMENTS

The authors would like to acknowledge Sally Samora for her efforts in fabricating the binary optics. This work performed at Sandia National Laboratories supported by the U. S. Department of Energy under contract number DE-AC04-94AL85000.

9 REFERENCES

[1] D. R. Neal, T. J. O'Hern, J. R. Torczynski, M. E. Warren and R. Shul, "Wavefront sensors for optical diagnostics in fluid mechanics: application to heated flow, turbulence and droplet evaporation," *SPIE* **2005**, pp. 194-203 (1993).

[2] D. W. Hanson, "Wavefront sensors for turbulence correction", *SPIE* **351**, pp. 104-107 (1983).

[3] J. G. Allen, A. Jankevics, D. Wormell, and L. Schmutz, "Digital wavefront sensor for astronomical image compensation," *SPIE* **739**, pp. 124-128 (1987).

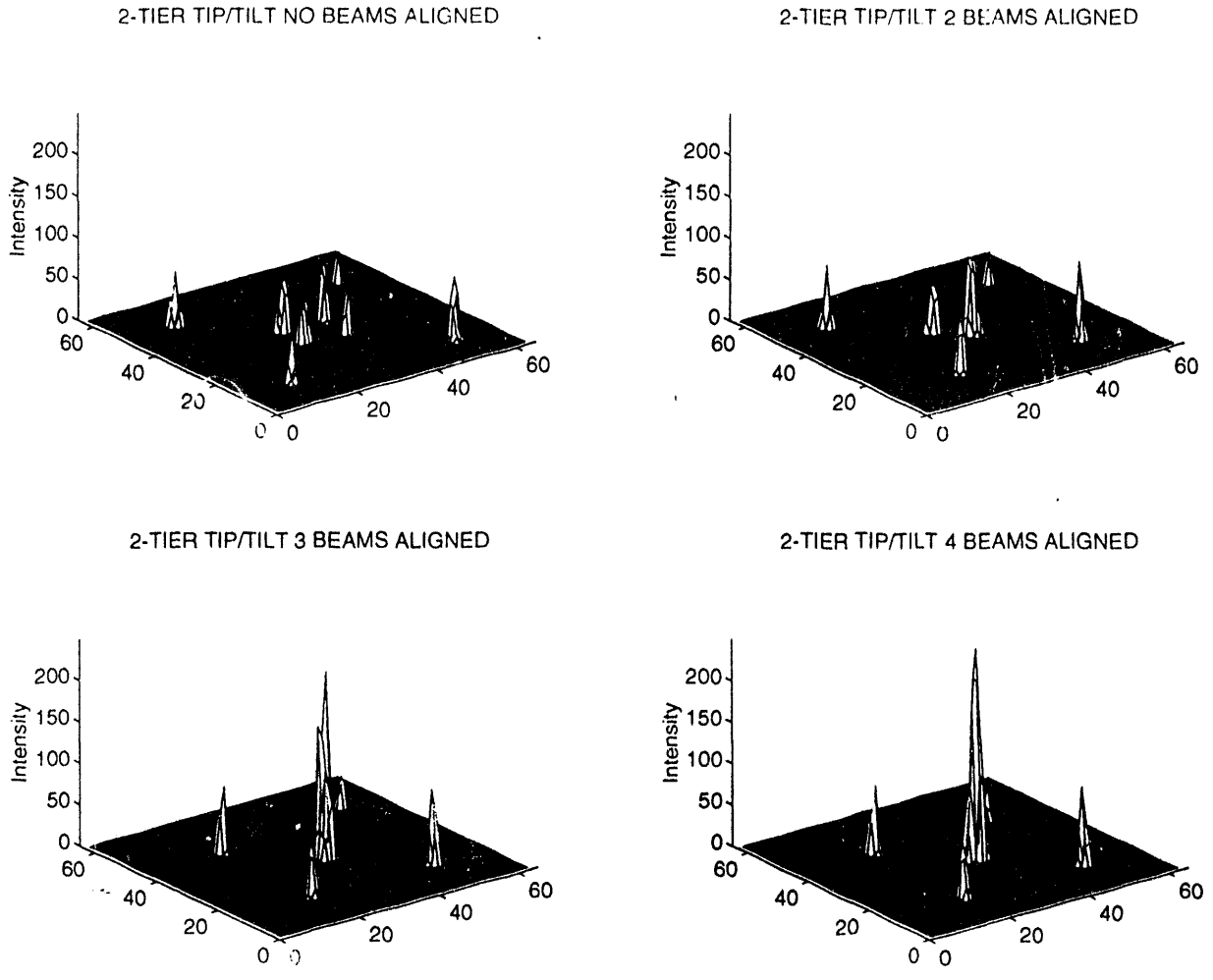

Figure 16: Measured far-field patterns from a two-tier lenslet array.

[4] M. Tarabocchia, S. Holly, and D. Jungwirth, "Active intracavity alignment system using a dynamic Hartmann sensor approach," *SPIE* **251**, pp. 100-106 (1980).

[5] D. S. Acton and R. C. Smithson, "Solar astronomy with a 19-segment adaptive mirror," *SPIE* **1542**, pp. 159-164 (1991).

[6] R. A. Hutchin, "Combined shearing interferometer and Hartmann wavefront sensor," U. S. Patent 4,518,854 (21 May 1985).

[7] H. E. Tomaschke and R. R. Rice, "Integrated optical wavefront sensor", *SPIE* **578**, pp. 228-232 (1985).

[8] G. Rousset, J-C. Fontanella, P. Kern, P. Lena, P. Gigan, F. Rigaut, J-P. Gaffard, C. Boyer, P. Jabourel, and F. Merkle, "Adaptive optics prototype system for infrared astronomy, I: System description," *SPIE* **1237**, pp. 336-344 (1990).

[9] D. Kwo, G. Damas, W. Zmek, "A Hartmann-Shack wavefront sensor using a binary optic lenslet array," *SPIE* **1544**, pp. 66-74 (1991).

[10] E. P. Wallner, "Comparison of wavefront sensor configurations using optical reconstruction and correction," *SPIE* **351**, pp. 42-53 (1983).

[11] R. M. Gagliardi, "Optimal post detection phase estimation for wavefront sensing," *SPIE* **351**, pp. 34-41 (1983).

[12] W. H. Southwell, "Wave-front estimation from - wavefront slope measurements," *JOSA* **70** (8), pp. 998-1006 (August 1980).

[13] D. D'Amato, and R. Centamore, "Two applications for microlens arrays: detector fill factor improvement and laser diode collimation," *SPIE* **1544**, pp. 166-171 (1991).

[14] H. W. Lau, N. Davies, M. McCormick, "Microlens array fabricated in surface relief with high numerical aperture," *SPIE* **1544**, pp. 178-188 (1991).

[15] K-H. Brenner, "Techniques for integrating 3D-optical systems," *SPIE* **1544**, pp. 263-270 (1991).

[16] D. R. Neal, T. G. Smith, G R. Eisler, J. L. Wilcoxen, and R. R. Rosenthal "Multiple laser beam combining and phasing using closed-loop control," *SPIE* **1920**, pp. 9–19 (1993).

[17] A. Lazzarini, G. H. Ames, "Algebraic multigrid method applied to the hierarchical control of a segmented active mirror," *SPIE* **2121**, (1994).

[18] E. G. Johnson, A. D. Kathman, D. H. Hochmuth, A. Cook, D. R. Brown, and B. Delaney, "Advantages of genetic algorithm optimization methods in diffractive optic design," *SPIE* **CR49**, pp. 54-74 (1993).

[19] W. B. Veldkamp and G. J. Swanson, "Developments in Fabrication of Binary Optical Elements," *SPIE* **437**, pp. 54-59 (1983).

[20] J. A. Cox, T. Werner, J. Lee S. Nelson, B. Fritz, and J. Bergstrom, "Diffraction efficiency of binary optical elements," *SPIE* **1211**, pp. 116-124 (1990).

[21] R. K. Tyson, "Measuring phase errors of an array or segmented mirror with a single far- field intensity distribution," *SPIE* **1542**, pp. 62-75 (1991).

[22] N. C. Mehta, and C. W. Allen, "Remote alignment of segmented mirrors with far-field optimization," *Appl. Opt.* **31**(30) (1992).

[23] N. C. Mehta, and C. W. Allen, "Segmented mirror alignment with far-field optimization in the presence of atmospheric turbulence," *Appl. Opt.* **32**(15) (1993).

[24] N. C. Mehta, and C. W. Allen, "Dynamic compensation of atmospheric turbulence with far-field optimization," *JOSA A* **11**(1), pp. 434-443 (1994).

[25] T. S. McKechnie, "Atmospheric turbulence and the resolution limits of large ground-based telescopes," *JOSA A* **9**(11), pp. 1937-1954 (1992).

[26] The MathWorks, Inc., *MATLAB*, ver. 4.0, Natick, MA (1993).

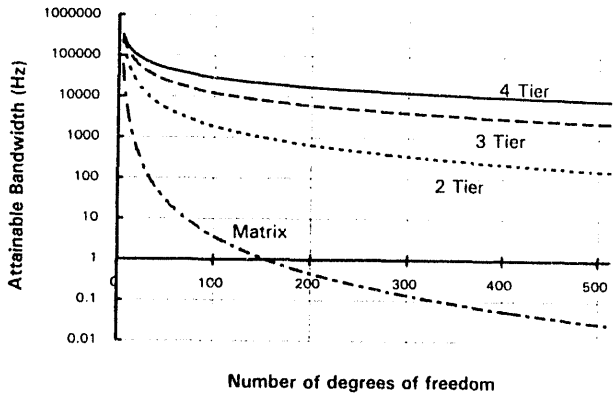

Figure 17: Attainable bandwidth for an adaptive optics system using hierarchical control.

[14] H. W. Lau, N. Davies, M. McCormick, "Microlens array fabricated in surface relief with high numerical aperture," *SPIE* **1544**, pp. 178-188 (1991).

[15] K-H. Brenner, "Techniques for integrating 3D-optical systems," *SPIE* **1544**, pp. 263-270 (1991).

[16] D. R. Neal, T. G. Smith, G. R. Eisler, J. L. Wilcoxen, and R. R. Rosenthal "Multiple laser beam combining and phasing using closed-loop control," *SPIE* **1920**, pp. 9–19 (1993).

[17] A. Lazzarini, G. H. Ames, "Algebraic multigrid method applied to the hierarchical control of a segmented active mirror," *SPIE* **2121**, (1994).

[18] E. G. Johnson, A. D. Kathman, D. H. Hochmuth, A. Cook, D. R. Brown, and B. Delaney, "Advantages of genetic algorithm optimization methods in diffractive optic design," *SPIE* **CR49**, pp. 54-74 (1993).

[19] W. B. Veldkamp and G. J. Swanson, "Developments in Fabrication of Binary Optical Elements," *SPIE* **437**, pp. 54-59 (1983).

[20] J. A. Cox, T. Werner, J. Lee, S. Nelson, J. Fritz, and J. Bergstrom, "Diffraction efficiency of binary optical elements," *SPIE* **1211**, pp. 116-124 (1990).

[21] R. K. Tyson, "Measuring phase errors of an array or segmented mirror with a single far- field intensity distribution," *SPIE* **1542**, pp. 62-75 (1991).

[22] N. C. Mehta, and C. W. Allen, "Remote alignment of segmented mirrors with far-field optimization," *Appl. Opt.* **31**(30) (1992).

[23] N. C. Mehta, and C. W. Allen, "Segmented mirror alignment with far-field optimization in the presence of atmospheric turbulence," *Appl. Opt.* **32**(15) (1993).

[24] N. C. Mehta, and C. W. Allen, "Dynamic compensation of atmospheric turbulence with far-field optimization," *JOSA A* **11**(1), pp. 434-443 (1994).

[25] T. S. McKechnie, "Atmospheric turbulence and the resolution limits of large ground-based telescopes," *JOSA A* **9**(11), pp. 1937-1954 (1992).

[26] The MathWorks, Inc., *MATLAB*, ver. 4.0, Natick, MA (1993).

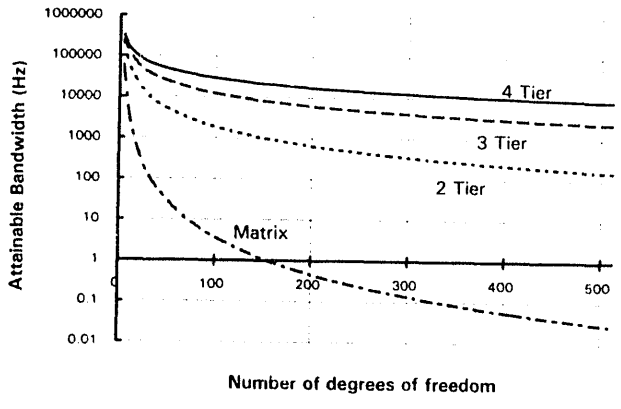

Figure 17: Attainable bandwidth for an adaptive optics system using hierarchical control.

DATE
FILMED
6/2/94
END